nature communications

Article

https://doi.org/10.1038/s41467-025-63079-w

Caudate serotonin signaling during social exchange distinguishes essential tremor and Parkinson's disease patients

Received: 21 March 2025

Accepted: 8 August 2025

Published online: 02 September 2025

Check for updates

Alec E. Hartle[1,11] ✉, Kenneth T. Kishida[2,3,4,11], L. Paul Sands[5,11], Seth R. Batten[5], Leonardo S. Barbosa[5], Dan Bang[5,6], Terry Lohrenz[5], Jason P. White[5], Arian K. Sohrabi[3], Rebecca L. Calafiore[4], Alexandra G. DiFeliceantonio[5,7], Adrian W. Laxton[4], Stephen B. Tatter[4], Mark R. Witcher[5,8], P. Read Montague[5,9,10,12] ✉ & W. Matt Howe[1,12] ✉

Dynamic changes in dopamine, noradrenaline, and serotonin release are believed to causally contribute to the neural computations that support reward-based decision making. Accordingly, changes in signaling by these systems are hypothesized to underwrite multiple cognitive and behavioral symptoms observed in many neurological disorders. Here, we characterize the release of these neurotransmitters measured concurrently in the caudate of patients with Parkinson's disease or essential tremor undergoing deep brain stimulation surgery as they played a social exchange game. We show that violations in the expected value of monetary offers are encoded by opponent patterns of dopamine and serotonin release in essential tremor, but not Parkinson's disease, patients. We also demonstrate that these changes in serotonin signaling comprise a neurochemical boundary that subsegments these two neuromotor diseases. Our combined results point to a neural signature of altered reward processing that can be used to understand the signaling deficiencies that underwrite these diseases.

Parkinson's disease (PD) and essential tremor (ET) collectively affect ~7.2 million people in the United States[1,2]. The symptoms of each disorder are believed to emerge in large part because of aberrant patterns of brain activity, though they are clinically distinct and have been hypothesized to reflect distinct underlying neuro-pathologies. For example, PD is a progressive disorder that is associated with bradykinesia, rigidity, and resting tremor[3,4]. In addition to these motor pathologies, PD is also associated with a number non-motor symptoms, including sleep disruptions, increased vulnerability to neuropsychiatric disorders, as well as deficits in cognitive functions like attentional control and decision making[4–9].

One of the biological hallmarks of PD is the loss of dopaminergic (DA) neurons in the substantia nigra pars compacta (SNc)[10,11], though it is increasingly recognized coincident disruptions in other monoamine neurotransmitter systems (e.g., serotonin; 5HT, noradrenaline; NA) also contribute to disease symptoms[12,13]. For example, reduced concentrations of 5HT and its metabolites have been observed in both the cerebral spinal fluid and postmortem brain samples from PD patients,

[1]School of Neuroscience, Virginia Tech, Blacksburg, VA, USA. [2]Department of Biology, Wake Forest University, Winston-Salem, NC, USA. [3]Department of Translational Neuroscience, Wake Forest University School of Medicine, Winston-Salem, NC, USA. [4]Department of Neurosurgery, Wake Forest University School of Medicine, Winston-Salem, NC, USA. [5]Fralin Biomedical Research Institute, Virginia Tech, Roanoke, VA, USA. [6]Center of Functionally Integrative Neuroscience, Aarhus University, Aarhus, Denmark. [7]Department of Human Nutrition, Foods, and Exercise, Virginia Tech, Blacksburg, VA, USA. [8]Division of Neurosurgery, Virginia Tech Carilion School of Medicine, Roanoke, VA, USA. [9]Department of Physics, Virginia Tech, Blacksburg, VA, USA. [10]Wellcome Centre for Human Neuroimaging, University College London, London, UK. [11]These authors contributed equally: Alec E. Hartle, Kenneth T. Kishida, L. Paul Sands. [12]These authors jointly supervised this work: P. Read Montague, W. Matt Howe. ✉e-mail: aleceh@vt.edu; read@vtc.vt.edu; wmhowe@vt.edu

with preferential declines in innervation of the caudate nucleus of the dorsal striatum[14–16], which correlate with the severity of both motor and non-motor symptoms of the disorder[14,17]. There is also evidence to suggest that brain-wide noradrenergic signaling is disrupted in PD[18], stemming from the degeneration of NA neurons of the locus coeruleus that may precede the well characterized changes in SNc DA populations[19–21]. Though often linked to sleep disruptions common in PD[22,23], these changes in NA release capacity may also contribute to deficits in cognitive function and affective reactivity[20,24,25].

In contrast to PD, a defining feature of ET is limb tremors that manifest predominantly during movement[26,27]. ET has historically been assumed to be purely a motor disorder, though notably, patients with ET have been found to be at increased risk for mild cognitive impairment and dementia[28–30]. Notably, these alterations in cognitive function tend to be more pronounced in individuals with late-onset disease, and manifest more selectively in executive functions like attentional control and language[29–31]. At the level of neural circuits affected in ET, changes in GABAergic signaling within the cerebellum are believed to lead to aberrant patterns of activity along relays between cerebellar Purkinje cells and motor thalamus, leading to altered recruitment of motor cortex ensembles and disrupted motor control[32,33]. Growing evidence also suggests that changes in excitatory balance within the cerebellum can also seed deficits in attentional function[34] as well as language processing[35] observed in ET. Further supporting the distinct neural pathways associated with these motor diseases, the pronounced decline in DA activity within the dorsal striatum associated with PD, which can even be detected in prodromal phases of the disorder, is not observed in patients with ET[36]. Indeed, whereas all monoamine systems are impacted by PD, they appear to be relatively spared in ET, except for possible local cerebellar changes in 5HT receptor function that may account for previous reports of exacerbated motor symptoms following 5HT agonist treatments in ET patients[26,37–39].

Even though PD and ET emerge as a result of distinct neural circuit abnormalities, both patient groups routinely undergo awake-deep brain stimulation (DBS) surgery to manage motor symptoms[40,41]. The most common clinical target for DBS in PD is the subthalamic nucleus[42] and for ET is the ventral intermediate nucleus of the thalamus[43]. For each of these targets, the trajectory of the clinical DBS electrodes passes through the caudate nucleus of the dorsal striatum, a nexus of aberrant monoaminergic activity in PD patients. Furthermore, striatal monoamine signaling, in particular DA and 5HT release, is hypothesized to play a mediatory role in the same domains of reward-based decision-making that have been described in PD patients[44–47]. We have developed a machine learning-enhanced approach to electrochemistry that can be deployed during DBS surgery[44,48–53], validated both in vitro and in vivo using optogenetics in rodents[52–54]. This method grants us a window of opportunity provided by DBS surgery to measure changes in DA, NA, and 5HT concurrently, with sub-second temporal resolution (10 Hz), and spatial granularity (μm) in the brains of conscious humans. Here, we utilized this approach to gain insight into two major questions: (1) the regulation of DA, NA, and 5HT release in the human caudate during reward evaluation; and (2) how such reward-related monoamine release varies between patients with these two distinct neurological diseases. To probe caudate monoamine function, we had patients perform a monetary social exchange game, a task which previous studies have shown recruits striatal circuits, including the caudate[55]. Furthermore, similar socially based decision-making tasks have been shown to be sensitive to changes in brain monoamine concentrations[56,57] and recruit monoamine release in other parts of the basal ganglia[52]. Therefore, we reasoned that this task, combined with our technique, would provide a context to explore disease-related alterations in the functional recruitment of ascending DA, NA, and 5HT systems. Our combined results reveal disease-specific patterns of reward-evoked monoamine release that may provide insight into the neurochemistry that underwrites these two prevalent motor disorders.

Results

Experimental design

Here, we characterized DA, NA, and 5HT release in individuals with PD ($n = 12$) or ET ($n = 6$). Patients undergoing DBS surgery had a carbon fiber microelectrode placed in the caudate for electrochemical recordings by the neurosurgeon during the procedure. They then performed a two person "take-it-or-leave-it" ultimatum game (UG), which is a well-tested social exchange task that probes players' responses to "fair" and "unfair" monetary offers[58]. In our version of UG, two players are involved: one proposes how to split $20 (e.g., $10/$10 split), and the other decides to accept or reject the offer (Fig. 1a). All patients in our study played the role of the responder and were presented with 30 offers from a hypothetically human partner through a monitor. Each trial started with a partner screen to indicate a new proposer was playing, and although not explicitly stated, offers were randomly generated from Gaussian distributions. Offers were presented in two blocks of 15 trials, starting with offers that were on average low ($\mu = \$4$, $\sigma = 1.5$) and transitioned to a block with high mean offers ($\mu = \$10$, $\sigma = 1.5$), or vice versa (Fig. 1b, c). In 60% of trials, participants were asked to rate how they felt about the offer.

Previous data suggests ascending monoamine systems, in particular DA and 5HT, are critical for broadcasting prediction errors, or the difference between expected and received outcomes[47,59]. Therefore, we used a validated Bayesian ideal observer model[55] to characterize players' shifting expectations of offer amounts across the task. The model allowed us to operationalize the difference between the expected "norm" and "actual" offer on each trial as a normed prediction error (NPE) value, with positive (Pos) NPEs representing offers greater than expected and negative (Neg) NPEs representing offers less than expected (Supplementary Fig. 1a, b and Fig. 1d, e).

Behavioral results

At the level of behavior, we noted that the time to decide to accept or reject offers was similar between NPEs and patient groups (Linear mixed-effects model, B-M1: Patient Group × NPE interaction, $F(1, 555.12) = 1.79$, $p = 0.18$; Supplementary Table 1 and Fig. 1c). As expected, offers with negative NPEs were rejected more frequently (B-M2: main effect of NPE, $F(1, 17) = 41.11$, $p = 6.44 \times 10^{-6}$), and this was consistent between patient groups (B-M2: main effect of Patient Group, $F(1, 17) = 0.45$, $p = 0.51$; Fig. 1d). Further, patients in general reported feeling happier during trials with offers higher than expected compared to offers lower than expected (B-M3: main effect of NPE, $F(1, 323.69) = 144.30$, $p = 9.7 \times 10^{-28}$; Fig. 1f); and again, this pattern was similar between PD an ET patients (B-M3: main effect of Patient Group, $F(1, 17.29) = 0.02$, $p = 0.88$, Supplementary Fig. 1e, f).

Neurochemical results

To assess the relationship between neurotransmitter release and the encoding of positive and negative NPEs[50,52,59–61], we focused our analyses on the time around offer presentation. Specifically, we estimated DA, NA, and 5HT concentrations every 100 ms to derive a times series of each neurotransmitter for each trial (see Batten et al. [53], Online Methods; Fig. 1g–i). We then extracted the area under the curve (AUC) from a 4 s window starting at offer presentation on each trial and used linear mixed-effects models to test whether these AUC values varied as a function of neurotransmitter identity (DA, NA, 5HT), NPE type (positive or negative), and patient group (see Supplementary Table 2 for full results for models N-M1:M6). We found that neurotransmitter concentrations during offer presentation indeed varied as a function of NPE type (Linear mixed-effects model, N-M1: Neurotransmitter × NPE interaction, ($F(2, 1669.02) = 4.58$, $p = 0.01$), and these effects were distinct between patient groups (N-M1: Neurotransmitter × NPE × Patient Group interaction, ($F(2, 1669.02) = 3.86$, $p = 0.021$).

Focusing on each patient group alone, in ET patients, positive and negative NPEs were distinguished by different patterns of release across

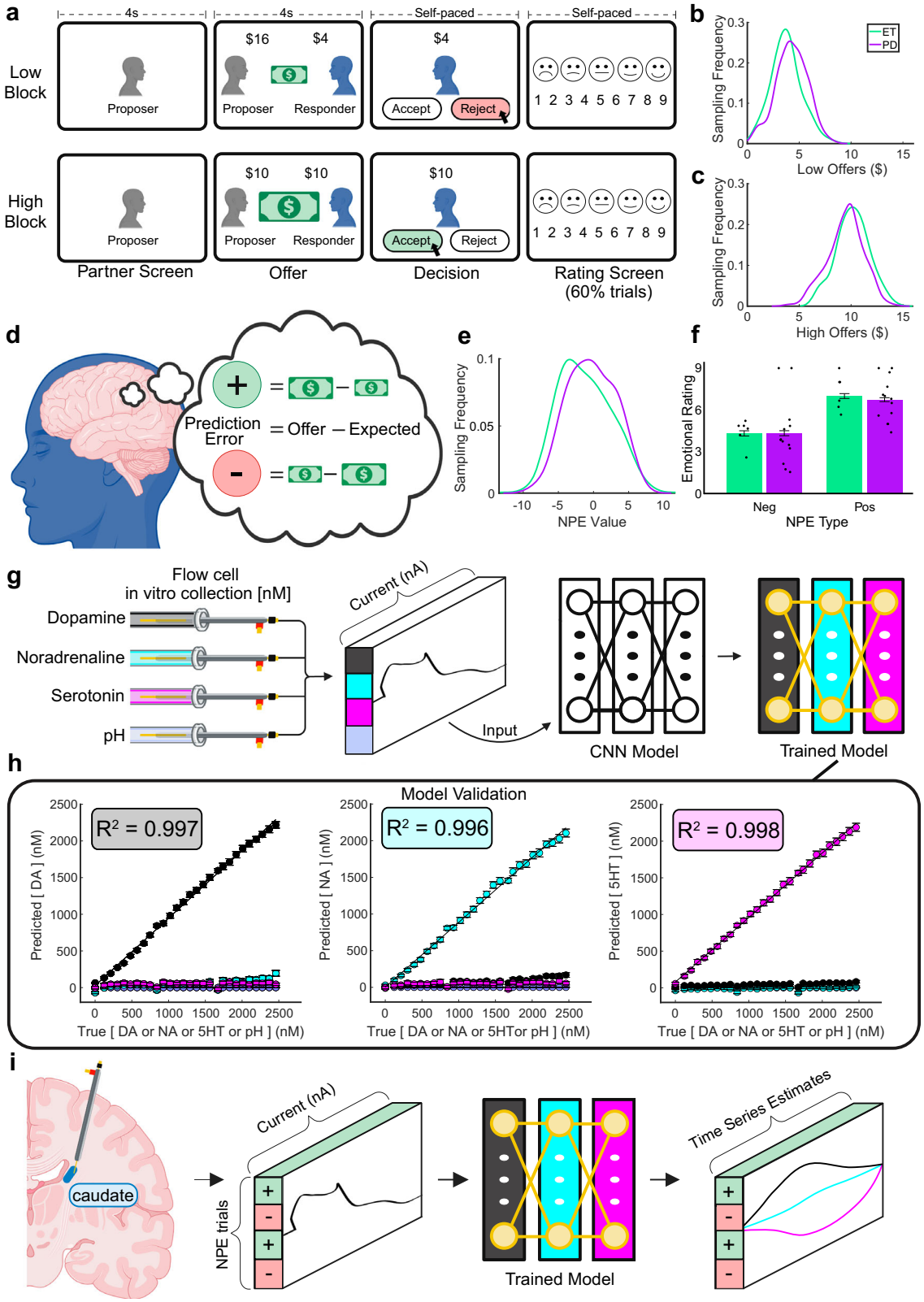

neurotransmitters (Fig. 2a–c; N-M2: Neurotransmitter × NPE interaction; $F(2, 526.01) = 6.28$, $p = 0.002$). Positive NPEs were associated with robust increases in DA and decreases in 5HT relative to negative NPEs (Bonferroni corrected post-hoc tests; DA Pos. vs. Neg NPE, $t(531) = 2.239$, $p = 0.026$; 5HT Pos vs. Neg NPE; $t(531) = -2.692$, $p = 0.007$). In contrast, there were no significant patterns in DA or 5HT responses during positive or negative NPE offers in PD patients (Fig. 2d–f; N-M3: Neurotransmitter × NPE interaction $F(2, 1143.01) = 0.18$, $p = 0.84$). We then focused on each neurotransmitter alone and compared AUCs between patient groups and prediction errors. In looking at the response of DA, we found there was a difference between positive and negative NPE trials, with DA release on average being higher on positive NPE trials (N-M4: main effect of NPE $F(1, 558.31) = 4.01$, $p = 0.046$), and while DA patterns were not present in PD patients (e.g., Fig. 2f), patient

Fig. 1 | Experimental design and electrode model. a Illustration of the ultimatum game. **b** Distribution of low offers ($USD) between essential tremor (ET, mint green) and Parkinson's disease (PD, lavender) groups. **c** Distribution of high offers between groups. **d** Illustration of norm prediction error (NPE) calculation. **e** Distribution of NPE values between groups. **f** Average emotional ratings to positive (Pos) and negative (Neg) NPEs between groups. Bar plots presented as mean ± SEM and black dots are indivdual patient means (ET, $n = 6$; PD, $n = 12$). **g** Illustration of prediction model training. From left to right, electrode recordings from in vitro monoamine concentrations are input into a convolutional neural network (CNN) to create a trained model. **h** Tenfold cross validation plots for dopamine (DA), noradrenaline (NA), and serotonin (5HT). Model root mean square error: DA, 35.4745 nanomolar (nM); NA, 42.2127 nM; 5HT, 23.1238 nM. Dots presented as mean ± standard error of the mean. **i** Illustration of in vivo recording and monoamine concentration estimations. From left to right, electrode recordings in the caudate are input into our trained model and time series estimates are outputted and separated by NPE type. **a**, **d**, **g**, and **i** were created in BioRender.

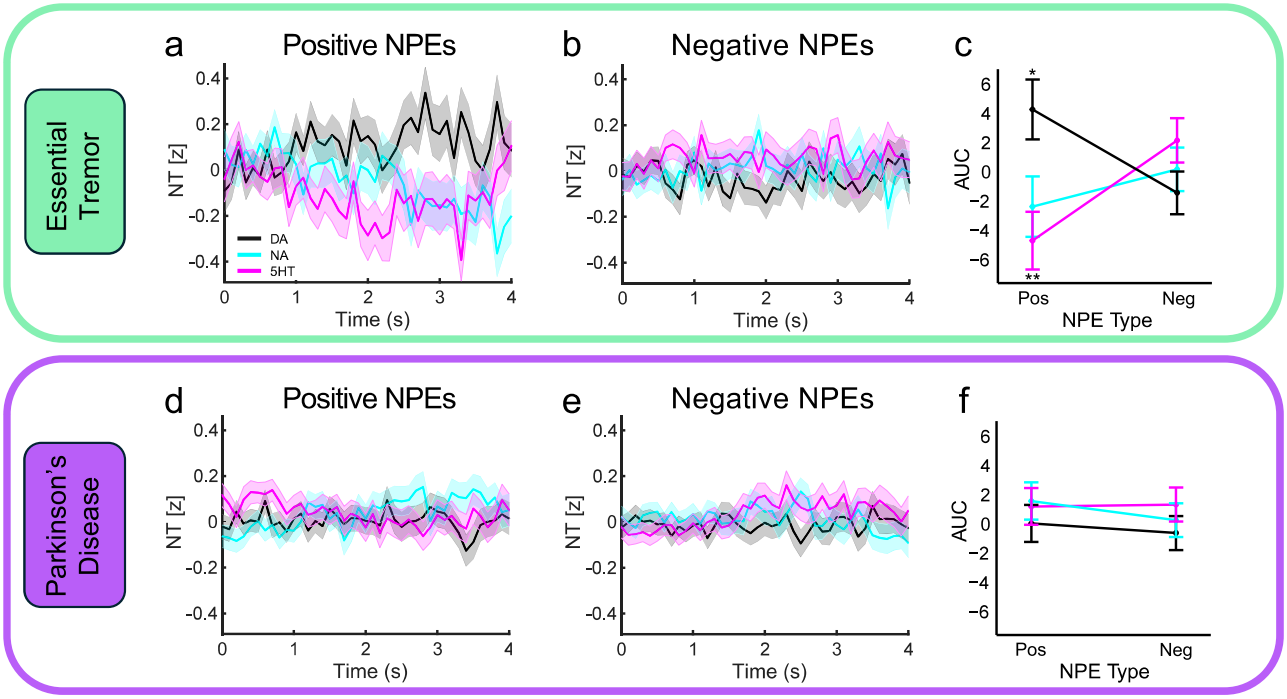

Fig. 2 | Monoamine signaling separates disease states in caudate. a Dopamine (DA, black), noradrenaline (NA, cyan), and serotonin (5HT, magenta) responses in patients with essential tremor (ET, mint green, $n = 6$) to positive (Pos) and **b** negative (Neg) NPEs. **c** Line plots for mean area under the curve (AUC, 4 s window) of neurotransmitter responses to Pos and Neg NPEs. Bonferroni corrected post-hoc tests were performed following linear mixed-effects model (N-M2; DA Pos. vs. Neg NPE, $t(531) = 2.239$, $p = 0.026$; 5HT Pos vs. Neg NPE; $t(531) = -2.692$, $p = 0.007$). **d** Time series estimates from patients with Parkinson's disease (PD, lavender, $n = 12$) during Pos and **e** Neg NPEs. **f** Line plots of AUCs for PDs during Pos and Neg NPEs. **a**–**f** Data represented as trial-level mean ± standard error of the mean.

group differences in DA were not statistically robust ($p > 0.05$). Notably, the differences in 5HT responses appeared more robust, and the overall reduction in 5HT on positive NPEs observed in ETs was absent in PDs (N-M5: NPE × Patient Group interaction for 5HT; $F(1, 545.01) = 4.46$, $p = 0.035$; 5HT response on positive NPE, ET vs. PD $t(81.3) = -2.281$, Bonferroni corrected $p = 0.025$). Of note, there were no significant fluctuations in NA release associated with positive or negative NPEs in either patient population (N-M6: all p's > 0.05), supporting the general hypothesis that DA and 5HT are the primary drivers of prediction error encoding in the caudate.

Importantly, there are many sources of variability in our patient groups that could contribute to the group-level differences in neurotransmitter release described above. To unpack this finding, we ran additional linear mixed-effects models to determine if our results could be explained by electrode placement within the caudate (Supplementary Figs. 2–4), medication status (Supplementary Tables 3 and 4), PD clinical features (Supplementary Table 5), or subgroups defined by rejection rates (Supplementary Fig. 5). Importantly, none of these variables accounted for the neurotransmitter responses described above for ET or PD patient groups (all $p > 0.05$). Together, the above analysis revealed a distinct profile of monoamine release in these two disease states as uncovered by a social exchange task.

Serotonin signaling distinguishes patient groups

Our results suggested that patterns of caudate monoamine release dynamics in response to monetary offers may represent a neurochemical boundary between PD and ET patient groups. We next sought to assess whether these diseases-specific patterns of NPE-evoked neurotransmitter release were sufficient to separate the patient groups. To that end, we performed a singular value decomposition (SVD) on the DA, NA, and 5HT changes during offer presentation (AUC values as above), and found latent dimensions (singular vectors, SV) which separated ETs and PDs. These latent dimensions (SV weights) were dominated by 5HT and DA NPE responses relative to NA. Projecting ET and PD patients into 2-dimensional space defined by singular vectors 1 and 3 revealed a partition between patient groups (logistic classifier; 86% accuracy, $p = 0.04$). Notably, patient labels were not included in the SVD computation and did not contribute to this separation. Given this separation between patient groups revealed by the above, we went back to our AUC data and assessed the relationship between each patient's DA, NA, and 5HT estimates during positive and negative NPEs. Whereas NA showed nearly complete overlap between the two patient groups, the relationships between 5HT and DA release on positive and negative NPEs unveiled a marked separation between ETs and PDs (88% accuracy, $p = 0.03$). Importantly, this distinction was

apparent in patients both on and off antidepressant medications, which target monoamine transport proteins (Supplementary Tables 3 and 4). Next, we performed permutation testing of the logistic regressions to predict disease state (ET = 1, PD = 0) based on each of the NPE AUC and singular vectors (i.e., "SVD-regression") to get a better sense of the uniqueness of their apparent ability to separate the disease groups. We performed 10,000 permutation tests of each logistic regression model with the disease state labels shuffled. These tests indicated that 5HT NPE AUCs drive this separation (See Supplementary Table 6 for statistical results of the regression permutation tests). In fact, 5HT positive NPE responses alone are sufficient to predict disease state (i.e., AUC of ROC curve is 0.82, $p = 0.03$). Combined, while ET and PD patients differed with respect to the pattern of DA and 5HT release in response to positive and negative NPEs, the differences in 5HT were key in distinguishing these two motor diseases.

Discussion

We have provided evidence that monoamine release in the caudate, evoked by violations of expected monetary offer amounts, can distinguish ET and PD patients. 5HT responses, not DA or NA, evoked by NPEs emerged as the key factor in separating ETs from PDs, highlighting the need for further research into the role of 5HT dysfunction in PD. In patients with ET, DA and 5HT exhibited an opponent relationship, with DA increasing and 5HT decreasing when offers exceeded expectations. The importance of DA-5HT opponency during reward-related processing has previously been proposed[62,63]; with fast changes in DA release generally linked to the prediction of rewards and increases in 5HT release associated with an expectation of punishment[64,65]. Given the ability of 5HT release to directly inhibit DA release[66], these two systems are often cast as the substrates of distinct, but interacting, appetitive and aversive computations. However, the literature around the shared and unique information encoded by DA and 5HT is conflicting, with some studies reporting DA release following the omission of aversive outcomes[67] and increases in 5HT neuronal activity in response to appetitive reward-predictive cues[68]. New advancements in imaging techniques available for model organisms have only recently confirmed the presence of DA and 5HT opponency in the striatum in mice, specifically showing that coincident increases in DA and decreases in 5HT in the striatum causally contribute to Pavlovian cue-reward associations[47]. Our data suggest that this pattern of opponency in DA and 5HT release also underwrites human social exchanges, specifically in the context of a positive NPEs. While further research is needed to determine the precise cognitive operations indexed by this pattern of DA and 5HT release, our studies suggest that alterations in such neurochemical coordination may ultimately be key to understanding the etiology of cognitive and behavioral impairments associated with PD. We acknowledge variability in the overall signal change on a given error-type between patients in each group, but a strikingly consistent relationship between the magnitude of DA, NA, and 5HT release on positive and negative NPEs. These data suggest that while there is individual variation in the extent to which DA, NA, and 5HT systems are "tuned" to either positive or negative prediction errors, the relationship between neurochemical responses on the two NPE types is more constrained. These findings highlight the need for further research into sources of individual variation in NPE sensitivity, as well as the possible existence of an extrinsic neural circuit that mediates the way each is encoded by ascending systems.

Several factors should be acknowledged that may have influenced our results. For one, in our cohort, we found no evidence that the distinction between ET and PD neurotransmitter responses reflected differences in electrode positioning between groups (Supplementary Figs. 2–4). However, given the evidence for regional differences in striatal neurotransmission previously observed in model species[69–71], it is possible that the DA and 5HT release dynamics described here are unique to the caudate recording site in these studies. Future studies are needed to determine if the topographic patterns of monoamine release described in the rodent striatum extend to humans. Additionally, it is not currently possible to perform the experiments described here in healthy human controls. Therefore, we cannot unequivocally state that our results from the ET cohort reflect "normal" signaling. However, given the lack of evidence suggesting broad monoaminergic dysfunction in ET (Elias & Shah, 2024; Gerber & Lynd, 1998; Gironell et al., 2012; Jiménez-Jiménez et al., 2020; Sommer et al., 2004), we believe these data offer needed insight into the neurochemistry of human cognition. It is also important to acknowledge that PD is a heterogeneous disorder, and disease duration as well as patient-specific symptomologies may reflect a similar heterogeneity in monoaminergic dysfunction[72–75]. As reported, within our PD cohort, we found no evidence for unique patterns of monoamine signaling based on their clinical features, or how long they had been diagnosed with PD (Supplementary Table 5), although it remains possible that as more data from these patients accumulates, patterns of release corresponding to different manifestations of PD may emerge. Indeed, our current sample size is smaller than many cognitive neuroscience studies in healthy participants, and future work should seek to replicate, or refine, the results in larger sample sizes. However, we note that our sample is typical for studies using intraoperative recordings in patients, and previous studies using human electrochemistry have identified robust results at the single-subject level[44] as well as in cohorts smaller than those in the current study[54]. Finally, given how the ultimatum game naturally engages emotional processing through violating the players' expectations, it is possible that the absence of DA-5HT opponency in PD reflects a disease-specific change in emotional engagement with the task. That said, we found no difference between groups in emotional ratings to positive or negative NPEs, pointing to a similar level of emotional capture between groups (Fig. 1f). We additionally found no evidence that antidepressant medication status impacted our main results (Supplementary Tables 3 and 4).

Combined, the signaling discrepancies described above likely represent underlying differences in the regulation of cognitively evoked DA and 5HT release between ET and PD patients. These findings highlight a boundary based on neurochemical signaling that clearly dissociates ET and PD patients and provides the foundation for future studies investigating coordinated neurotransmitter release patterns that support human decision making.

Methods

Ethics and recruitment

This study complies with all ethical regulations and was approved by Institutional Review Boards at Wake Forest University Health Sciences (IRB00017138) and Virginia Tech (11-078). Before surgery, patients provided written and informed consent. Once consent was obtained, the instructions of the ultimatum game were described. Patients were told they would be compensated with a payment up to $60 based on their performance in the game and that one round would be picked randomly and be added as a bonus payment. Base payments ranged from $50–$60 for each task session, however, patients were not informed of the base payment. Six patients with essential tremor (one female, mean age ± SD = 56 ± 9.5 years) and 12 patients with Parkinson's disease (one male played twice during two separate DBS surgeries, four females, mean age ± SD = 59.4 ± 11.4 years) participated in the ultimatum game experiment (see Supplementary Table 3).

Behavioral testing

Ultimatum game. Participants played as responders and were informed that a "partner" would be proposing the monetary splits. Sessions were blocked with two conditions: high or low offers (Fig. 1a). Either the first 15 trials were high offers and the last 15 trials were low offers, or low offers were in the first block and high offers in the second block (ET: low-to-high $n = 4$, high-to-low $n = 2$; PD: low-to-high $n = 3$, high-to-low $n = 10$). Unknown to the participants, the offers were

randomly generated from Gaussian distributions with low mean $4 and high mean $10 with a standard deviation of $1.5 (Actual offer mean ± SD: ET, low $3.75 ± 1.42 and high $10.14 ± 1.55; PD, low $4.27 ± 1.48, and high $9.45 ± 1.73). For each trial, the game started with a partner screen to indicate a new proposer was playing (partner screen locked for 4 s). Then the offer screen came on, which showed the proposed split between the proposer and responder (offer screen locked for 4 s). After the offer screen, the decision screen was displayed, and the responder was asked to accept or reject the offer (self-paced). On 60% of the trials, a rating screen was shown in which the responder was asked to rate their feelings about the offer on a scale of one to nine, with a one being sad and nine being happy (self-paced). Lastly, a blank screen was displayed before a new trial was initiated (screen locked for 2–4 s). The game was controlled by custom written software using HTML and JavaScript, which displayed the game to the participants and logged the behavioral events for neural data alignment.

Electrochemical approach

Data acquisition. The carbon fiber electrodes used for in vivo and in vitro data collection were fabricated in-house as previously described[44,48–50,52,53]. Voltammetric current was obtained while participants underwent DBS. The scanning protocol was established from previous human[44,48–50,52,53] and rodent work[76,77]. Measurements were taken at 10 Hz and consisted of a 10 ms triangular voltage ramp (from −0.6 V to +1.4 V then back to −0.6 V at 400 V/s) and then held at −0.6 V for 90 ms before the next ramp. The current response was sampled at 100 kHz. Prior to recording, we first applied a 60 Hz precycling protocol to our measurement triangle waveform to equilibrate the electrode in the brain. Voltammetric recordings were done using Axon Instruments (MultiClamp 700B Patch Clamp Amplifier, Digidata 1550B Data Acquisition System, CV 7B-EC headstage) from Molecular Devices (Molecular Devices, LLC, San Jose, CA, 95134).

In vitro data collection. Seventy-six carbon fiber electrodes were used to collect in vitro data to train our model[53]. Each in vitro electrode had four datasets collected, one dataset per analyte (dopamine, noradrenaline, serotonin, and pH). For each monoamine, the dataset consisted of 30 separate concentration vectors and ranged from 0 to 2500 nM (pH ~7.4). Additionally, each dataset contained five mixtures of all three monoamines ranging from 840 to 1690 nM (pH ~7.4). The fourth dataset consisted of phosphate-buffered saline (PBS) solutions of varying pH (7.0–7.8) with 5 additional sets that included varying neurotransmitter concentrations. A small subset of the electrodes received different concentration vectors within the same ranges or had more than four analytes collected on them. Monoamine order and concentration vectors were randomized for each electrode. Before data was collected, the electrodes were placed horizontally within a flow cell to submerge the carbon fiber and reference in PBS solution and then pre-cycled at 97 Hz for 10 min. After pre-cycling, we began data collection on the concentration vectors by first running 97 Hz precycle for 27 s, followed by 65 s of our 10 Hz sample protocol. To reduce variation caused by equilibrium and electrical noise, we focused on the most stable 15 s window of the 10 Hz recording.

In vitro model training. Changes in monoamine concentrations were predicted from in vivo current measurements by ensembles of convolutional neural networks trained from our in vitro data. We adapted the deep convolutional neural network InceptionTime model[78] for time series classification to support multivariate regression on our in vitro datasets. We implemented equally weighted averages from in vivo concentration predictions through multi-InceptionTime models, similarly to Fawaz et al.[78]. We coded the model in Python and used Keras[79] and TensorFlow[80]. Our InceptionTime network was based on two ResNet[81] blocks, each block containing 3 convolutional blocks, and each convolutional block consisted of 4 parallel convolutional layers. Each layer was composed of 32 filters, with progressively increasing kernel sizes (1, 10, 20, 40). The outputs of each convolutional layer were combined, followed by the application of batch normalization and RELU activations. This output was processed through a bottleneck convolutional layer with a kernel size of one and 32 filters and provided input to the subsequent convolutional block. To implement the ResNet architecture, the input first passed through a bottleneck convolutional layer with a kernel size of 1 and 32 filters. This output was then added to the result of the first ResNet block. After activation, the output from the first ResNet block served as the input to the second ResNet block and the operation was repeated. Finally, after global average pooling, the output of the second ResNet block was passed through a dense layer with four output nodes, providing predictions for the four analytes. All models employed mean squared error as the loss function. The training process utilized the ADAM optimizer[82], starting with an initial learning rate of 1e-3, which was halved after 5 consecutive epochs without a reduction in validation loss with no set minimum learning rate. The model that corresponded to the epoch with the lowest validation loss was chosen as the final model for that training run.

To train the model, 70 electrodes were used, and 6 electrodes were randomly selected to be held out for model testing. For every electrode used to train the model, 150 current sweeps were taken for each unique concentration vector combination. The training set consisted of 1,170,150 sweeps from 2594 unique concentration vector combinations. The test set, derived from the 6 held-out electrodes, consisted of 135,450 sweeps from 803 unique concentration vector combinations. The model was produced from a mixture of experts and final predictions were averaged from a 20-ensemble training run. For each ensemble, the datasets were split, such that 90% of the data was used for training and 10% used for validation. The data was divided by electrode-concentration, ensuring that all data points for a specific concentration from a given electrode were grouped together in the same set. The labels were then z-scored within each analyte. After the training process, we applied the inverse normalization procedure to the model predictions generated from new current inputs and the models underwent training for 35 epochs. We then carried out a ten-fold cross validation test for the prediction model using all 76 in vitro electrodes. For every electrode in the test fold, the model trained on the remaining nine folds to produce x and y points, where true analyte concentrations are x and predicted analyte concentrations are y (Fig. 1h). For each validation plot, we used x and y pairs for the analyte being considered, and for the other analytes in the plot, we used x and e, where e represents the error (e = estimate−true). For DA, 5HT, and NA, we binned all x-values into 28 equally spaced bins and computed the average estimated analyte values or error values for each probe. Within each bin, we averaged the x-values and either the predicted analyte values or errors across probes and plotted those pairs. Probe number was used as degree of freedom to calculate error bars.

In vivo neurotransmitter predictions. Final predictions for in vivo data were produced using a mixture of experts approach. This involved training an ensemble of models with the same hyperparameters and averaging their predictions. Variations in weights due to initialization, the order in which data was fed during training, and the stochastic descent algorithm introduced differences in the convergence of each model. Different validation sets were employed in each run to mitigate overfitting. The in vivo current traces were differentiated in the same manner as during training and then evaluated by each model. The concentration estimates were obtained by averaging the predictions from the ensemble of models.

Analysis

Data handling. To align behavior to the time series neurochemical estimates of dopamine, noradrenaline, and serotonin, we used MATLAB (MathWorks, Natick, MA). Each neurotransmitter was aligned

to the offer reveal (7 s window, 3 s before offer, and 4 s after the offer, in which patient was locked-in before decision was possible). Each neurotransmitter trace per trial was first linearly detrended and then causally smoothed by a 0.5 s window across the 7-s snippet. For each snippet, the mean and standard error of the mean was calculated across the 7-s snippet for each neurotransmitter per trial and then each trial was z-scored across the entire snippet. AUC was then computed from the 4 s post-onset of the offer.

Bayesian observer model. We assumed participants believed that offers were generated from a normal distribution, but were uncertain about its mean and variance, and updated their estimates of these parameters trial by trial using Bayesian inference. Concretely, the distribution of offers conditional on the mean the μ and variance σ^2 is given by:

$$p(s|\mu,\sigma^2) = \text{Normal}(\mu,\sigma^2)$$

The prior over μ and σ^2 in trial i + 1 is taken as the posterior after trial *i*. We selected a conjugate prior, so that the form remained the same across trials (see the exposition in Gelman et al.[83]; also Xiang et al.[55] and Gu et al.[84]). More precisely, the prior was given by

$$p(\mu,\sigma^2) = p_1(\mu|\sigma^2)p_2(\sigma^2)$$

with

$$p_1(\mu|\sigma^2) = \text{Normal}\left(\hat{\mu}, \frac{\sigma^2}{k}\right)$$

$$p_2(\sigma^2) = \text{Inv}-\chi^2\left(\hat{\sigma}^2, \nu\right).$$

Here, $\hat{\mu}, \hat{\sigma}^2$, and ν are hyperparameters. $\text{Inv}-\chi^2$ is the scaled inverse-chi-squared distribution. The hyperparameters for trial $i+1$ are given in terms of the trial *i* offer s_i hyperparameters by

$$k_{i+1} = k_i + 1 \quad \nu_{i+1} = \nu_i + 1$$

$$\hat{\mu}_{i+1} = \hat{\mu}_i + \frac{1}{k_i+1}(s_i - \hat{\mu}_i)$$

$$\nu_{i+1}\hat{\sigma}^2_{i+1} = \nu_i\hat{\sigma}^2_i + \frac{k_i}{k_{i+1}}(s_i - \hat{\mu}_i)^2$$

Note that the expected offer $E_i[S_i]$ on trial *i* is $\hat{\mu}_i$, so that

$$\text{Norm prediction error} = \delta_i = s_i - E_i[S_i] = s_i - \hat{\mu}_i$$

$$\text{Positive norm prediction error} = \max(\delta_i, 0),$$

$$\text{Negative norm prediction error} = \max(-\delta_i, 0).$$

We took the initial values of the hyperparameters for trial 1 to be $\hat{\mu}_1 = 10$, $\hat{\sigma}^2_1 = 4$, $k_1 = 4$, and $\nu_1 = 10$. After norm prediction errors were calculated using participants' offer sequences, trial-level AUC measurements were categorized by positive and negative errors.

Statistical analysis

We used linear mixed-effects models for the analysis of behavioral and neural data effects with a random effect of subject. Males and females were included in both patient groups; however, given that our study sample is determined by clinical need, this study was not designed to assess sex differences in neurotransmitter release, and biological sex was not a factor in our statistical models. The function lmer() in R (R Core Team, 2024) was used to compute all linear mixed-effects models. Type III ANOVA was then run on each linear mixed-effects model and pairwise comparisons on the estimated marginal means (Bonferroni corrected) were used to explore significant main effects and interactions.

Linear mixed-effects analyses. Denoted in Wilkinson notation:

Behavioral data statistics

B-M1, Reaction time ~ 1 + Patient Group × NPE + (1 | subject)
B-M2, Rejection rate ~ 1 + Patient Group × NPE + (1 | subject)
B-M3, Emotional rating ~ 1 + Patient Group × NPE + (1 | subject)

Neural data statistics

N-M1, $AUC_{DA/NA/5HT}$ ~ 1 + Neurotransmitter × NPE × Patient Group + (1 | subject)
N-M2, AUC_{ET} ~ 1 + Neurotransmitter × NPE + (1 | subject)
N-M3, AUC_{PD} ~ 1 + Neurotransmitter × NPE + (1 | subject)
N-M4, AUC_{DA} ~ 1 + Patient Group × NPE + (1 | subject)
N-M5, AUC_{5HT} ~ 1 + Patient Group × NPE + (1 | subject)
N-M6, AUC_{NA} ~ 1 + Patient Group × NPE + (1 | subject)

Singular vector decomposition, logistic classifiers, and permutation testing

To analyze the neurotransmitter patterns of activity, SVD was applied to the mean AUC values from dopamine, noradrenaline, and serotonin during positive and negative norm prediction errors. The AUC data from each group were concatenated into a single matrix where rows represented subjects and columns corresponded to the difference in mean neurotransmitter estimate under positive and negative NPEs. Additionally, we performed a series of logistic regression analyses to determine the predictive accuracy of each monoamine NPE AUC vector and right singular vector for classifying ET patients versus PD patients, which we computed as the area under the receiver operator characteristic curve (AUROC) for each model. To assess the statistical significance of each logistic classifier, we adopted a nonparametric approach and performed 10,000 permuted logistic regression per singular vector, with each permutation involving a random shuffling of the disease class label. We computed *p*-values associated with each NPE and singular vector's AUROC value by dividing the number of permutation tests with AUROC values greater than or equal to the actual AUROC value by the total number of permutations.

Reporting summary

Further information on research design is available in the Nature Portfolio Reporting Summary linked to this article.

Data availability

The data generated in this study have been deposited on GitHub: https://github.com/AlecHartle/article-UG-Caudate.

Code availability

The code used in this study have been deposited on GitHub: https://github.com/AlecHartle/article-UG-Caudate.

References

1. Marras, C. et al. Prevalence of Parkinson's disease across North America. *NPJ Parkinsons Dis.* **4**, 21 (2018).
2. Louis, E. D. & Ottman, R. How many people in the USA have essential tremor? Deriving a population estimate based on epidemiological data. *Tremor Other Hyperkinet. Mov.* **4**, 259 (2014).
3. Hughes, A. J., Daniel, S. E., Kilford, L. & Lees, A. J. Accuracy of clinical diagnosis of idiopathic Parkinson's disease: a clinico-pathological study of 100 cases. *J. Neurol. Neurosurg. Psychiatry* **55**, 181–184 (1992).
4. Sveinbjornsdottir, S. The clinical symptoms of Parkinson's disease. *J. Neurochem* **139**, 318–324 (2016).

5. Williams-Gray, C. H., Foltynie, T., Brayne, C. E., Robbins, T. W. & Barker, R. A. Evolution of cognitive dysfunction in an incident Parkinson's disease cohort. *Brain* **130**, 1787–1798 (2007).
6. Robbins, T. W. & Cools, R. Cognitive deficits in Parkinson's disease: a cognitive neuroscience perspective. *Mov. Disord.* **29**, 597–607 (2014).
7. Albin, R. L. et al. Cholinergic systems, attentional-motor integration, and cognitive control in Parkinson's disease. *Prog. Brain Res.* **269**, 345–371 (2022).
8. Williams-Gray, C. H., Foltynie, T., Lewis, S. J. G. & Barker, R. A. Cognitive deficits and psychosis in Parkinson's disease. *CNS Drugs* **20**, 477–505 (2006).
9. Onofrj, M., Thomas, A. & Bonanni, L. New approaches to understanding hallucinations in Parkinson's disease: phenomenology and possible origins. *Expert Rev. Neurother.* **7**, 1731–1750 (2007).
10. Cardoso, F. et al. A statement of the MDS on biological definition, staging, and classification of Parkinson's disease. *Mov. Disord.* **39**, 259–266 (2024).
11. Damier, P., Hirsch, E. C., Agid, Y. & Graybiel, A. M. The substantia nigra of the human brain. II. Patterns of loss of dopamine-containing neurons in Parkinson's disease. *Brain* **122**, 1437–1448 (1999).
12. Halliday, G. M., Blumbergs, P. C., Cotton, R. G., Blessing, W. W. & Geffen, L. B. Loss of brainstem serotonin- and substance P-containing neurons in Parkinson's disease. *Brain Res.* **510**, 104–107 (1990).
13. Zarow, C., Lyness, S. A., Mortimer, J. A. & Chui, H. C. Neuronal loss is greater in the locus coeruleus than nucleus basalis and substantia nigra in Alzheimer and Parkinson diseases. *Arch. Neurol.* **60**, 337–341 (2003).
14. Tohgi, H., Abe, T., Takahashi, S., Takahashi, J. & Hamato, H. Alterations in the concentration of serotonergic and dopaminergic substances in the cerebrospinal fluid of patients with Parkinson's disease, and their changes after L-DOPA administration. *Neurosci. Lett.* **159**, 135–138 (1993).
15. Kerenyi, L. et al. Positron emission tomography of striatal serotonin transporters in Parkinson disease. *Arch. Neurol.* **60**, 1223–1229 (2003).
16. Kish, S. J. et al. Preferential loss of serotonin markers in caudate versus putamen in Parkinson's disease. *Brain* **131**, 120–131 (2008).
17. Niccolini, F. et al. Loss of phosphodiesterase 10A expression is associated with progression and severity in Parkinson's disease. *Brain* **138**, 3003–3015 (2015).
18. Rommelfanger, K. S. et al. Norepinephrine loss produces more profound motor deficits than MPTP treatment in mice. *Proc. Natl. Acad. Sci. USA* **104**, 13804–13809 (2007).
19. Braak, H. et al. Staging of brain pathology related to sporadic Parkinson's disease. *Neurobiol. Aging* **24**, 197–211 (2003).
20. Espay, A. J., LeWitt, P. A. & Kaufmann, H. Norepinephrine deficiency in Parkinson's disease: the case for noradrenergic enhancement. *Mov. Disord.* **29**, 1710–1719 (2014).
21. Paredes-Rodriguez, E., Vegas-Suarez, S., Morera-Herreras, T., De Deurwaerdere, P. & Miguelez, C. The noradrenergic system in Parkinson's disease. *Front Pharm.* **11**, 435 (2020).
22. Uchiyama, M. et al. Incidental Lewy body disease in a patient with REM sleep behavior disorder. *Neurology* **45**, 709–712 (1995).
23. Sommerauer, M. et al. Evaluation of the noradrenergic system in Parkinson's disease: an 11C-MeNER PET and neuromelanin MRI study. *Brain* **141**, 496–504 (2018).
24. Remy, P., Doder, M., Lees, A., Turjanski, N. & Brooks, D. Depression in Parkinson's disease: loss of dopamine and noradrenaline innervation in the limbic system. *Brain* **128**, 1314–1322 (2005).
25. Del Tredici, K. & Braak, H. Dysfunction of the locus coeruleus-norepinephrine system and related circuitry in Parkinson's disease-related dementia. *J. Neurol. Neurosurg. Psychiatry* **84**, 774–783 (2013).
26. Elias, W. J. & Shah, B. B. Essential tremor. *JAMA* **332**, 418–419 (2024).
27. Elias, W. J. & Shah, B. B. Tremor. *JAMA* **311**, 948–954 (2014).
28. Lombardi, W. J., Woolston, D. J., Roberts, J. W. & Gross, R. E. Cognitive deficits in patients with essential tremor. *Neurology* **57**, 785–790 (2001).
29. Thawani, S. P., Schupf, N. & Louis, E. D. Essential tremor is associated with dementia: prospective population-based study in New York. *Neurology* **73**, 621–625 (2009).
30. Benito-León, J., Louis, E. D., Mitchell, A. J. & Bermejo-Pareja, F. Elderly-onset essential tremor and mild cognitive impairment: a population-based study (NEDICES). *J. Alzheimers Dis.* **23**, 727–735 (2011).
31. Janicki, S. C., Cosentino, S. & Louis, E. D. The cognitive side of essential tremor: what are the therapeutic implications?. *Ther. Adv. Neurol. Disord.* **6**, 353–368 (2013).
32. Louis, E. D. Essential tremor: evolving clinicopathological concepts in an era of intensive post-mortem enquiry. *Lancet Neurol.* **9**, 613–622 (2010).
33. Choe, M. et al. Purkinje cell loss in essential tremor: random sampling quantification and nearest neighbor analysis. *Mov. Disord.* **31**, 393–401 (2016).
34. Mannarelli, D. et al. The cerebellum modulates attention network functioning: evidence from a cerebellar transcranial direct current stimulation and attention network test study. *Cerebellum* **18**, 457–468 (2019).
35. Mariën, P. & Borgatti, R. Language and the cerebellum. *Handb. Clin. Neurol.* **154**, 181–202 (2018).
36. Sommer, U. et al. Detection of presymptomatic Parkinson's disease: combining smell tests, transcranial sonography, and SPECT. *Mov. Disord.* **19**, 1196–1202 (2004).
37. Gerber, P. E. & Lynd, L. D. Selective serotonin-reuptake inhibitor-induced movement disorders. *Ann. Pharmacother.* **32**, 692–698 (1998).
38. Gironell, A. et al. Gaba and serotonin molecular neuroimaging in essential tremor: a clinical correlation study. *Parkinsonism Relat. Disord.* **18**, 876–880 (2012).
39. Jiménez-Jiménez, F. J., Alonso-Navarro, H., García-Martín, E. & Agúndez, J. A. G. An update on the neurochemistry of essential tremor. *Curr. Med. Chem.* **27**, 1690–1710 (2020).
40. Benabid, A. L., Pollak, P., Louveau, A., Henry, S. & de Rougemont, J. Combined (thalamotomy and stimulation) stereotactic surgery of the VIM thalamic nucleus for bilateral Parkinson disease. *Appl. Neurophysiol.* **50**, 344–346 (1987).
41. Benabid, A. L. et al. Long-term suppression of tremor by chronic stimulation of the ventral intermediate thalamic nucleus. *Lancet* **337**, 403–406 (1991).
42. Limousin, P. et al. Effect on Parkinsonian signs and symptoms of bilateral subthalamic nucleus stimulation. *Lancet* **345**, 91–95 (1995).
43. Vaillancourt, D. E., Sturman, M. M., Verhagen Metman, L., Bakay, R. A. & Corcos, D. M. Deep brain stimulation of the VIM thalamic nucleus modifies several features of essential tremor. *Neurology* **61**, 919–925 (2003).
44. Bang, D. et al. Sub-second dopamine and serotonin signaling in human striatum during perceptual decision-making. *Neuron* **108**, 999–1010.e1016 (2020).
45. Cools, R., Nakamura, K. & Daw, N. D. Serotonin and dopamine: unifying affective, activational, and decision functions. *Neuropsychopharmacology* **36**, 98–113 (2011).
46. Boureau, Y. L. & Dayan, P. Opponency revisited: competition and cooperation between dopamine and serotonin. *Neuropsychopharmacology* **36**, 74–97 (2011).
47. Cardozo Pinto, D. F. et al. Opponent control of reinforcement by striatal dopamine and serotonin. *Nature* **639**, 143–152 (2025).

48. Kishida, K. T. et al. Sub-second dopamine detection in human striatum. *PLoS ONE* **6**, e23291 (2011).
49. Kishida, K. T. et al. Subsecond dopamine fluctuations in human striatum encode superposed error signals about actual and counterfactual reward. *Proc. Natl. Acad. Sci. USA* **113**, 200–205 (2016).
50. Moran, R. J. et al. The protective action encoding of serotonin transients in the human brain. *Neuropsychopharmacology* **43**, 1425–1435 (2018).
51. Sands, L. P. et al. Subsecond fluctuations in extracellular dopamine encode reward and punishment prediction errors in humans. *Sci. Adv.* **9**, eadi4927 (2023).
52. Batten, S. R. et al. Dopamine and serotonin in human substantia nigra track social context and value signals during economic exchange. *Nat. Hum. Behav.* **8**, 718–728 (2024).
53. Batten, S. R. et al. Emotional words evoke region- and valence-specific patterns of concurrent neuromodulator release in human thalamus and cortex. *Cell Rep.* **44**, 115162 (2025).
54. Bang, D. et al. Noradrenaline tracks emotional modulation of attention in human amygdala. *Curr. Biol.* **33**, 5003–5010.e5006 (2023).
55. Xiang, T., Lohrenz, T. & Montague, P. R. Computational substrates of norms and their violations during social exchange. *J. Neurosci.* **33**, 1099–1108 (2013).
56. Crockett, M. J., Clark, L., Tabibnia, G., Lieberman, M. D. & Robbins, T. W. Serotonin modulates behavioral reactions to unfairness. *Science* **320**, 1739 (2008).
57. Crockett, M. J., Clark, L., Hauser, M. D. & Robbins, T. W. Serotonin selectively influences moral judgment and behavior through effects on harm aversion. *Proc. Natl. Acad. Sci. USA* **107**, 17433–17438 (2010).
58. Camerer, C. F. *Behavioral Game Theory: Experiments in Strategic Interaction* (Russell Sage Foundation, 2003).
59. Montague, P. R., Dayan, P. & Sejnowski, T. J. A framework for mesencephalic dopamine systems based on predictive Hebbian learning. *J. Neurosci.* **16**, 1936–1947 (1996).
60. Schultz, W., Dayan, P. & Montague, P. R. A neural substrate of prediction and reward. *Science* **275**, 1593–1599 (1997).
61. Hart, A. S., Rutledge, R. B., Glimcher, P. W. & Phillips, P. E. Phasic dopamine release in the rat nucleus accumbens symmetrically encodes a reward prediction error term. *J. Neurosci.* **34**, 698–704 (2014).
62. Redgrave, P. Modulation of intracranial self-stimulation behaviour by local perfusions of dopamine, noradrenaline and serotonin within the caudate nucleus and nucleus accumbens. *Brain Res.* **155**, 277–295 (1978).
63. Daw, N. D., Kakade, S. & Dayan, P. Opponent interactions between serotonin and dopamine. *Neural Netw.* **15**, 603–616 (2002).
64. Amo, R. et al. The habenulo-raphe serotonergic circuit encodes an aversive expectation value essential for adaptive active avoidance of danger. *Neuron* **84**, 1034–1048 (2014).
65. Dayan, P. & Huys, Q. Serotonin's many meanings elude simple theories. *Elife* **4**, e07390 (2015).
66. Alex, K. D. & Pehek, E. A. Pharmacologic mechanisms of serotonergic regulation of dopamine neurotransmission. *Pharm. Ther.* **113**, 296–320 (2007).
67. Kutlu, M. G., Tat, J., Christensen, B. A., Zachry, J. E. & Calipari, E. S. Dopamine release at the time of a predicted aversive outcome causally controls the trajectory and expression of conditioned behavior. *Cell Rep.* **42**, 112948 (2023).
68. Liu, Z. et al. Dorsal raphe neurons signal reward through 5-HT and glutamate. *Neuron* **81**, 1360–1374 (2014).
69. Mohebi, A., Wei, W., Pelattini, L., Kim, K. & Berke, J. D. Dopamine transients follow a striatal gradient of reward time horizons. *Nat. Neurosci.* **27**, 737–746 (2024).
70. Nakamura, K., Santos, G. S., Matsuzaki, R. & Nakahara, H. Differential reward coding in the subdivisions of the primate caudate during an oculomotor task. *J. Neurosci.* **32**, 15963–15982 (2012).
71. Brown, H. D., McCutcheon, J. E., Cone, J. J., Ragozzino, M. E. & Roitman, M. F. Primary food reward and reward-predictive stimuli evoke different patterns of phasic dopamine signaling throughout the striatum. *Eur. J. Neurosci.* **34**, 1997–2006 (2011).
72. Kwon, K. Y., Lee, H. M., Lee, S. M., Kang, S. H. & Koh, S. B. Comparison of motor and non-motor features between essential tremor and tremor dominant Parkinson's disease. *J. Neurol. Sci.* **361**, 34–38 (2016).
73. Prange, S. et al. Early limbic microstructural alterations in apathy and depression in de novo Parkinson's disease. *Mov. Disord.* **34**, 1644–1654 (2019).
74. Hezemans, F. H. et al. Noradrenergic deficits contribute to apathy in Parkinson's disease through the precision of expected outcomes. *PLoS Comput. Biol.* **18**, e1010079 (2022).
75. Thobois, S. et al. Parkinsonian apathy responds to dopaminergic stimulation of D2/D3 receptors with piribedil. *Brain* **136**, 1568–1577 (2013).
76. Clark, J. J. et al. Chronic microsensors for longitudinal, subsecond dopamine detection in behaving animals. *Nat. Methods* **7**, 126–129 (2010).
77. Phillips, P. E. M., Stuber, G. D., Heien, M. L. A. V., Wightman, R. M. & Carelli, R. M. Subsecond dopamine release promotes cocaine seeking. *Nature* **422**, 614–618 (2003).
78. Ismail Fawaz, H. et al. InceptionTime: finding AlexNet for time series classification. *Data Min. Knowl. Discov.* **34**, 1936–1962 (2020).
79. Chollet, F. et al. Keras. https://keras.io (2015).
80. Martín Abadi, A. A. et al. TensorFlow: large-scale machine learning on heterogeneous systems. Preprint at https://arxiv.org/abs/1603.04467 (2016).
81. He, K., Zhang, X., Ren, S. & Sun, J. Deep Residual Learning for Image Recognition. In *2016 IEEE Conference on Computer Vision and Pattern Recognition (CVPR)* pp. 770–778 (IEEE, 2016). https://doi.org/10.1109/CVPR.2016.90.
82. Kingma, D. P. & Ba, J. Adam: a method for stochastic optimization. Preprint at https://arxiv.org/abs/1412.6980 (2017).
83. Gelman, A., Carlin, J. B., Stern, H. S. & Rubin, D. B. *Bayesian Data Analysis, Second Edition*. (Chapman & Hall/CRC. A CRC Press Company Boca Raton London New York Washington, D.C., 2004).
84. Gu, X. et al. Necessary, yet dissociable contributions of the insular and ventromedial prefrontal cortices to norm adaptation: computational and lesion evidence in humans. *J. Neurosci.* **35**, 467–473 - (2015).

Acknowledgements

We are grateful to the patients who participated in this study. This work was supported by the National Institute of Health NIDDK R01DK141764 (A.G.D., W.M.H., P.R.M.), NIMH R01MH122948 (P.R.M.), NIMH R01MH124115 (P.R.M., K.T.K.), NIMH R01MH122512 (P.R.M.), NIMH R01MH132635 (P.R.M.), NIMH R01MH121099 (K.T.K.), NCATS KL2TR001421 (K.T.K.), NIDA R01DA048096 (K.T.K.), NINDS R01NS092701 (P.R.M., K.T.K.), the Lundbeck Foundation R368-2021-325 (D.B.), and the Red Gates Foundation (P.R.M). Panels within Fig. 1 were created in BioRender (Fig. 1a: https://biorender.com/gge1ha0, Fig. 1d: https://biorender.com/w5bx1i8, Fig. 1g: https://biorender.com/vgk5994, Fig. 1i: https://biorender.com/48ojejs).

Author contributions

Conceptualization, K.T.K., T.L., P.R.M., W.M.H., A.E.H.; Data analysis, A.E.H., L.P.S., S.R.B., L.S.B., D.B., J.P.W., A.K.S., R.L.C., A.G.D., P.R.M., W.M.H.; Data collection, K.T.K., R.L.C., A.W.L., S.B.T., M.R.W., A.K.S; Funding acquisition, K.T.K., P.R.M., A.G.D., W.M.H.; Writing, A.E.H., K.T.K., L.P.S., S.R.B., D.B., T.L., A.K.S., A.G.D., P.R.M., W.M.H.

Competing interests

The authors declare no competing interests.

Additional information

Supplementary information The online version contains supplementary material available at https://doi.org/10.1038/s41467-025-63079-w.

Correspondence and requests for materials should be addressed to Alec E. Hartle, P. Read Montague or W. Matt Howe.

Peer review information *Nature Communications* thanks the anonymous reviewer(s) for their contribution to the peer review of this work. A peer review file is available.